Coupling of four-wave mixing and Raman scattering by ground-state atomic coherence

Michał Parniak,* Adam Leszczyński, and Wojciech Wasilewski
Institute of Experimental Physics, Faculty of Physics, University of Warsaw, Pasteura 5, 02-093 Warsaw, Poland
(Received 2 February 2016; revised manuscript received 30 March 2016; published 16 May 2016)

We demonstrate coupling of light resonant to transition between two excited states of rubidium and long-lived ground-state atomic coherence. In our proof-of-principle experiment a nonlinear process of four-wave mixing is used to achieve light emission proportional to independently prepared ground-state atomic coherence. Strong correlations between stimulated Raman-scattering light heralding the generation of ground-state coherence and the four-wave mixing signal are measured and shown to survive the storage period, which is promising in terms of quantum memory applications. The process is characterized as a function of laser detunings.

DOI: 10.1103/PhysRevA.93.053821

I. INTRODUCTION

Off-resonant Raman scattering is a robust approach to light-atom interfaces. One of the methods is to induce spontaneous Stokes scattering in which pairs of photons and collective atomic excitations—a two-mode squeezed state—are created. These excitations can be stored and later retrieved in the anti-Stokes process [1,2]. This approach is commonly known to be a basic building block of the Duan-Lukin-Cirac-Zoller (DLCZ) protocol [3].

Typically rubidium and cesium have been used as atomic systems in both warm and cold atomic ensembles [4–6]. These systems are coupled to light at near-IR wavelengths, such as 795 and 780 nm for rubidium $D1$ and $D2$ lines. Coupling to new wavelengths holds a promise to greatly extend capabilities of quantum memories. This can be accomplished by nonlinear frequency conversion in the four-wave mixing (4WM) process using strong resonant nonlinearities in atoms thanks to transitions between excited states. Such processes have been used to demonstrate frequency conversion in rubidium [7–11] or to generate photon pairs in the cascaded spontaneous 4WM process [12–14]. Multiphoton processes are also a developing method to interface light and Rydberg atoms [15–17].

Chanelière *et al.* [14] proposed to combine the processes of Raman scattering and 4WM by first creating photon pairs in a cascaded spontaneous 4WM in one atomic ensemble and then storing photons as collective atomic excitations in another cold ensemble, and an experiment was recently realized [18]. As a result they obtained a two-mode squeezed state of atomic excitations and telecom photons. Another approach was to frequency-convert light generated in quantum memory with 4WM [19], in order to create a frequency-converted quantum memory. In all cases one atomic ensemble was used for storage and another for frequency conversion or photon generation.

In this paper we realize a Raman-like interface based on 4WM in warm rubidium vapors driven by ground-state atomic coherence. The process we present may be in principle used to generate correlated pairs of collective atomic excitations and photons coupled to transition between two excited states in a single, four-photon process in a single atomic ensemble. Transition between two excited states corresponds to 776-nm light as illustrated in Fig. 1(a). As the two intermediate states we use $5P_{3/2}$ and $5D_{5/2}$.

The paper is organized as follows. In Sec. II we discuss the principles behind our idea. In Sec. III we describe the experimental setup and methods we use to verify our findings. Finally, we give the results of our studies of the four-wave mixing interface, namely, correlations and statistical properties in Sec. IV A and detuning dependencies in Sec. IV B. We conclude the paper and give prospects for future developments in Sec. V.

II. GENERAL IDEA

In our experiment we generate ground-state atomic coherence ρ_{gh} and light denoted by 2Ph in a two-photon stimulated Raman Stokes process, seeded by vacuum fluctuations. The advantage of this approach is the fact that it is a well-established and effective way to prepare atomic ground-state coherence. In particular, it may be used in different regimes, starting from the single-photon and single-excitation spontaneous regime as in the DLCZ protocol [3,4] through the linear gain regime [20,21] and even in the nonlinear gain-saturation regime [22–24]. In the two latter cases, macroscopic ground-state coherence is generated [25]. The generated coherence and the number of scattered photons will be highly random but correlated. The atomic coherence is not averaged out to zero due to atomic motion, since the buffer gas makes the motion diffusive [26]. Moreover, the generated Raman field remains coherent with the driving field, so phase fluctuations of the driving field do not disturb the process [27]. In particular, the generated macroscopic ground-state coherence may be probed [28], may be read out [1], or may enhance further stimulated Raman process [29].

In this experiment, we observe concurrent generation of 776-nm light denoted by 4Ph in a four-photon process analogous to stimulated Raman scattering driven by ground-state coherence. It does not occur spontaneously in the macroscopic regime due to small gain. However, with macroscopic ρ_{gh} generated in the two-photon stimulated Raman process, the driving fields a, b, and c couple ground-state atomic coherence to the weak optical 4Ph field. In other words, the 4Ph process is stimulated by preexisting atomic coherence. In the leading order in drive beam fields Rabi frequencies Ω_i the atomic polarization resulting in emission of 4Ph signal

*michal.parniak@fuw.edu.pl

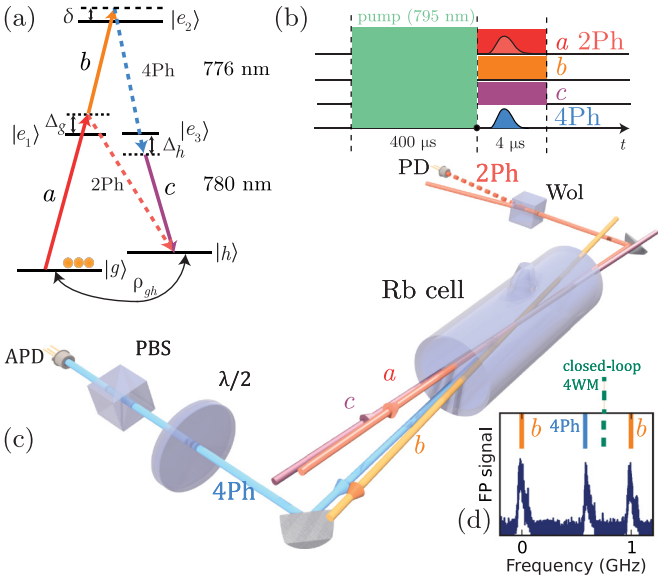

FIG. 1. (a) Configuration of atomic levels and fields we use to realize the four-photon interface, (b) pulse sequence used in the experiment, (c) the central part of the experimental setup demonstrating phase-matching geometry, and (d) trace of the 1-GHz FSR Fabry-Pérot interferometer signal showing the frequency of 4Ph field being different from what one would expect from the closed-loop process. Rows in panel (b) correspond to different beam paths presented in panel (c).

field is

$$\mathbf{P}_{4\mathrm{Ph}} = -n\mathbf{d}_{e_3e_2}\rho_{gh}\frac{\Omega_a\Omega_b\Omega_c^*}{4\Delta_g\delta\Delta_h}, \tag{1}$$

where n is the atom number density and $\mathbf{d}_{ij}$ are the dipole moments of respective transitions. From this formula it follows which detunings play a role.

For the experimental observation *a priori* knowledge of polarization properties is crucial. To find it, we add contributions from all possible paths through intermediate hyperfine states. Since the detunings from the intermediate $5P_{3/2}$ state are much larger than respective hyperfine splittings, we ignore the latter. The same approximation is adopted for the highest excited state $5D_{5/2}$. Even though the respective detuning δ is of the order of several MHz, similar to the hyperfine splitting of the highest excited state $5D_{5/2}$, the hyperfine structure is completely unresolved due to significant pressure broadening [30] in the 0.5 Torr krypton we use as buffer gas. Consequently, we may omit any detuning dependance and calculate the unnormalized polarization vector $\boldsymbol{\epsilon}$ of the signal light using the path-averaging formalism we developed in Ref. [9], by recalling the definitions of Rabi frequencies in Eq. (1):

$$\boldsymbol{\epsilon}_{4\mathrm{Ph}} \propto \sum_{F,\,m_F} \mathbf{d}_{e_3e_2}(\mathbf{E}_a\cdot\mathbf{d}_{ge_1}\mathbf{E}_b\cdot\mathbf{d}_{e_1e_2}\mathbf{E}_c^*\cdot\mathbf{d}_{e_3h}^*), \tag{2}$$

where $\mathbf{E}_i$ are electric fields of respective beams i. Summation is carried over all possible magnetic sublevels (F_i, m_{F_i}) of all intermediate states $|e_1\rangle$, $|e_2\rangle$, and $|e_3\rangle$.

III. EXPERIMENTAL METHODS

The experimental setup is built around the rubidium-87 vapor cell heated to 100 °C, corresponding to the atom number density $n = 7.5\times10^{12}$ cm^{-3} and the optical density of 1600 at the $D2$ line for the optically pumped ensemble. For the two lowest, long-lived states, we use two hyperfine components of the rubidium ground-state manifold, namely, $|5S_{1/2}, F=1\rangle = |g\rangle$ and $|5S_{1/2}, F=2\rangle = |h\rangle$. For the $|e_1\rangle$ and $|e_3\rangle$ states we take the hyperfine components of the $5P_{3/2}$ manifold, and for the highest excited state $|e_2\rangle$ we take those of the $5D_{5/2}$ manifold. Atoms are initially pumped into the $|g\rangle$ state using a 400-μs optical pumping pulse (at 795 nm). Next, three square-shaped driving pulses of 4-μs duration each are applied simultaneously, as shown in Fig. 1(b). Inside the cell, beams are collimated and have diameters of 400 μm, being well-overlapped over a 2-cm-long cylindrical region. They intersect at a small angle of 14 mrad, with 780-nm beams nearly counterpropagating with respect to the 776-nm beams, as presented in Fig. 1(c). Powers of the driving beams a, b, and c are 10, 45, and 8 mW, respectively.

The 780-nm two-photon Raman signal 2Ph copropagates with the driving field a. It is separated using a Wollaston polarizer (Wol) and detected on a fast photodiode (PD), with a 10^4 signal-to-driving-field leakage ratio. The four-photon signal 4Ph is emitted in the direction given by the phase-matching condition $\mathbf{k}_a + \mathbf{k}_b = \mathbf{k}_{4\mathrm{Ph}} + \mathbf{k}_c + \mathbf{K}$. The wave vector $\mathbf{K}$ of the spin-wave generated in the 2Ph process Raman scattering equals $\mathbf{K} = \mathbf{k}_a - \mathbf{k}_{2\mathrm{Ph}}$. We note that both longitudinal and transverse components of the spin-wave $\mathbf{K}$ are much smaller than those of light wave vectors, and consequently it has little effect on the 4Ph signal emission direction. This particular, nearly copropagating geometry allows us to couple the same spin-wave of wave vector $\mathbf{K}$ to both the 2Ph and 4Ph processes. In addition to the desired 4Ph signal, 776-nm light coming from the closed-loop process in which field c couples level $|e_3\rangle$ directly to $|g\rangle$ is emitted in the same direction [9] and at a frequency differing by only 6.8 GHz. However, when driving fields a, b, and c are x-, y-, and y-polarized, respectively, the 4Ph signal light is x-polarized, while the closed-loop 4WM light is y-polarized, where $x \perp y$. This arrangement enables filtering out the 4Ph signal from both stray 776-nm driving light and the closed-loop 4WM light with a polarizing beam-splitter (PBS, 10^2 extinction). To suppress the residual drive laser background at 780 nm the 4Ph signal goes through an interference filter (transmission of 80% for 776 nm and 10^{-3} for 780 nm) and is detected by an avalanche photodiode (APD). We were able to obtain a signal-to-background ratio of up to 10^2.

By rotating the half-wave plate ($\lambda/2$) we can easily switch between observing 4Ph and the closed-loop signal. For detunings optimal for the 4Ph process, we register less than 10 nW of the closed-loop 4WM light. The two signals display different temporal characteristics, also only 4Ph is correlated with the 2Ph light.

We verify the frequencies of 4Ph and the closed-loop light using a scanning Fabry-Pérot confocal interferometer of 1-GHz free spectral range (FSR) inserted in the 4Ph beam path. Figure 1(d) shows the trace obtained by scanning the interferometer for the detuning difference

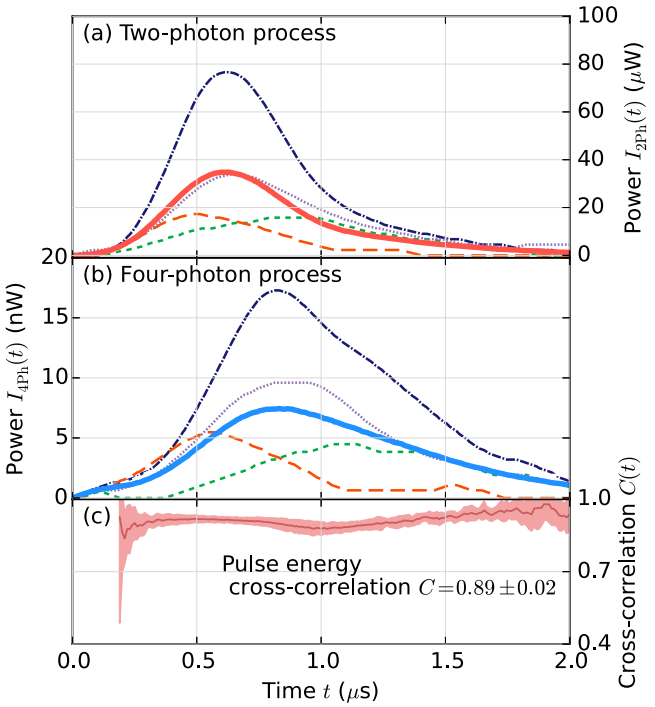

FIG. 2. (a, b) Averaged signal intensities (solid lines) with several single realizations (dashed lines), denoted by same colors in panels (a) and (b), demonstrating visible strong correlations. (c) Calculated cross correlation $C(t)$ between signals of four-photon (4Ph) and two-photon (2Ph) processes.

$\Delta_g + \Delta_h = 2\pi \times 3.43$ GHz. Leakage of the driving field b, induced by slight misalignment, is used as the frequency reference. The middle peak corresponds to the 4Ph signal, with a solid line indicating the expected frequency. The dashed line corresponds to the frequency one would expect from the closed-loop signal.

IV. RESULTS

A. Statistics and correlations

In our experiment we remain in the macroscopic scattered light intensity regime. When a strong Raman driving field is present, atoms are transferred to $|h\rangle$ simultaneously with scattering of 2Ph photons and buildup of large atomic coherence ρ_{gh}. The temporal shape of the 2Ph pulse is an exponential only at the very beginning, which we observe in Fig. 2(a). Not only the pulse energies but also the shapes fluctuate significantly from shot to shot, as the process is seeded by vacuum fluctuations [31]. However, the 4Ph pulse, presented in Fig. 2(b), nearly exactly follows the 2Ph pulse. We calculate temporal correlations between the 2Ph signal, which is known to be proportional to the ground-state atomic coherence ρ_{gh} and the 4Ph signal. The normalized intensity correlation at time t between the 2Ph signal $I_{2\mathrm{Ph}}(t)$ and the 4Ph signal $I_{4\mathrm{Ph}}(t)$ is calculated according to the formula $C(t) = \langle \Delta I_{2\mathrm{Ph}}(t) \Delta I_{4\mathrm{Ph}}(t) \rangle / \sqrt{\langle \Delta I^2_{2\mathrm{Ph}}(t) \rangle \langle \Delta I^2_{4\mathrm{Ph}}(t) \rangle}$ by averaging over 500 realizations, where the standard deviations $\langle \Delta I^2_{2\mathrm{Ph}}(t) \rangle$ and $\langle \Delta I^2_{4\mathrm{Ph}}(t) \rangle$ are corrected for electronic noise. Figure 2(c) presents the cross correlation $C(t)$. We observe that

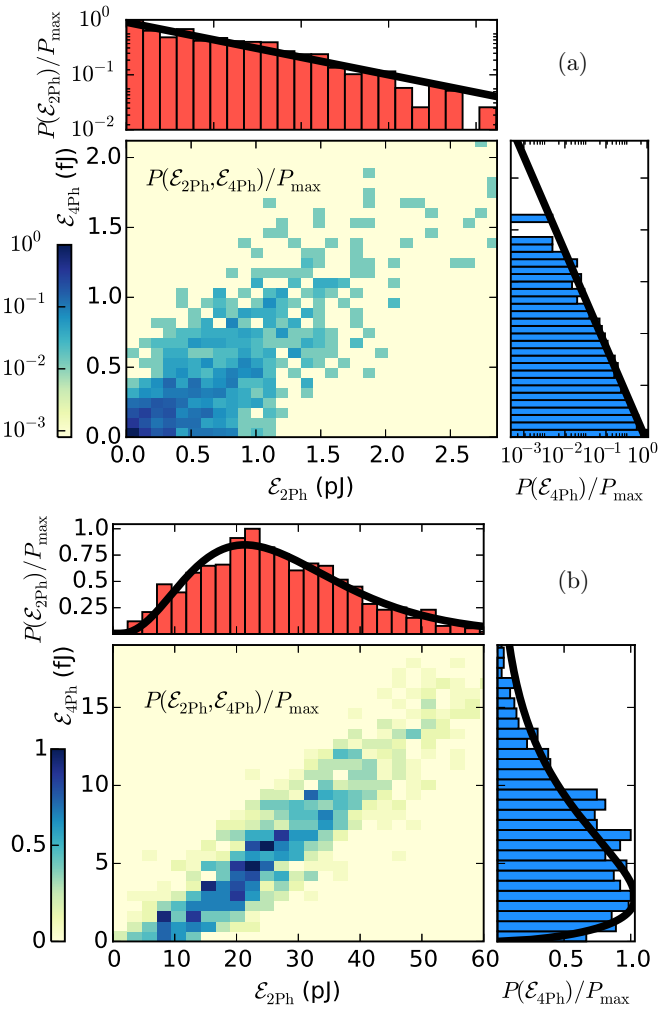

FIG. 3. Joint statistics $P(\mathcal{E}_{2\mathrm{Ph}},\mathcal{E}_{4\mathrm{Ph}})$ together with marginal distributions of registered pulse energies for (a) a short driving time of 200 ns, yield nearly single-mode thermal statistics (note the logarithmic scale in this plot), and (b) a longer driving time of 4 μs with observable pulse energy stabilization well described by multimode thermal statistics with a mode number $\mathcal{M}$ of 4.1 for 2Ph pulses and 1.6 for 4Ph pulses. Solid curves correspond to fitted thermal distributions.

correlations are high during the entire process, which proves that at any time both processes interact with the same atomic coherence ρ_{gh}, similarly as in some previous works on Λ-level configurations [28,32]. In particular, we are able to measure high correlation >0.9 at the very beginning of the pulses, where light intensities are low. This regime is quite promising for further quantum applications. To estimate the uncertainty of the calculated correlations, we divided the data into ten equal sets of 50 repetitions and calculated the correlation inside each set to finally obtain the uncertainty by calculating the standard deviation of the results from all the sets.

Next, we study the statistics and correlations of the pulse energies in detail. We consider short and long pulse duration regimes. Figure 3(a) corresponds to a short driving time of 200 ns. In this regime light generated in both the 2Ph and 4Ph processes is well-characterized by the single-mode thermal energy distribution $P(\mathcal{E}) = \langle \mathcal{E} \rangle^{-1} \exp(-\mathcal{E}/\langle \mathcal{E} \rangle)$ [33], where $\mathcal{E}$

is the total scattered light energy in a single realization. This observation shows that we excite only a single transverse-spatial mode, as intended by using a small size Raman driving beam a [21,34]. Thermal distribution yields very high pulse energy fluctuations (namely, the mean energy is equal to the standard deviation), which are due to vacuum fluctuations of the electromagnetic field and quantum fluctuations of the atomic state [22,35]. Still, we observe that the energies of the 2Ph and 4Ph pulses are highly correlated, which is demonstrated by the joint statistics $P(\mathcal{E}_{2\mathrm{Ph}},\mathcal{E}_{4\mathrm{Ph}})$. The residual spread is mainly due to the detection noise of both signals.

In the second regime [Fig. 3(b)] the driving pulses of 4 μs are longer than those in the previous scheme. The relative fluctuations become smaller due to gain saturation. We found the marginal statistics to be well described by multimode thermal distributions (with number of modes $\mathcal{M}$) given by

$$P(\mathcal{E}) = \frac{\mathcal{M}}{\langle\mathcal{E}\rangle\Gamma(\mathcal{M})}\left(\frac{\mathcal{E}\mathcal{M}}{\langle\mathcal{E}\rangle}\right)^{\mathcal{M}-1}\exp(-\mathcal{E}\mathcal{M}/\langle\mathcal{E}\rangle). \quad (3)$$

The joint statistics $P(\mathcal{E}_{2\mathrm{Ph}},\mathcal{E}_{4\mathrm{Ph}})$ demonstrate clear correlations, which are here less influenced by the detection noise than previously, as the pulse energies are higher.

Finally, we check that correlations are indeed mediated by ground-state atomic coherence by interrupting the scattering process for a dark period of $\tau = 450$ ns. This is proved by strong correlations between the intensities of light scattered before and after the dark period, observed in both 2Ph and 4Ph processes.

After the atoms are optically pumped as in the original scheme, we drive the processes with 150-ns pulses of the three driving fields a, b, and c. After a dark period of $\tau = 450$ ns, we drive the process for another 200 ns. The coherence ρ_{gh} generated in the first stage induces optical polarization at both the 4Ph field frequency [as in Eq. (1)] and the 2Ph field frequency:

$$\mathbf{P}_{2\mathrm{Ph}} = -n\mathbf{d}_{e_h e_1}\rho_{gh}\frac{\Omega_a}{\Delta_g}, \quad (4)$$

resulting in stimulated Raman emission. The full two-point correlation map presented in Fig. 4(b) is calculated as $C(t_1,t_2) = \langle\Delta I_{4\mathrm{Ph}}(t_1)\Delta I_{2\mathrm{Ph}}(t_2)\rangle/\sqrt{\langle\Delta I^2_{4\mathrm{Ph}}(t_1)\rangle\langle\Delta I^2_{2\mathrm{Ph}}(t_2)\rangle}$. Apart from the diagonal correlated areas at $t_1 \approx t_2 \approx 100$ and 800 ns, we observe the antidiagonal terms corresponding to correlations between the two pulses. Due to spontaneous emission and collisional dephasing all the excited atomic states decay quickly, with their lifetimes limited to 20 ns. This proves that we store information in the ground-state atomic coherence. The storage time τ is limited mainly by atomic motion. In fact, the stored ground-state coherence and in turn correlations decay in multiple ways, e.g., by diffusive spatial spread of atomic coherence [36,37] and by influx of optically pumped atoms into the interaction region. Finally, we mention that very similar results are obtained if the system is driven by the field a only in the first stage of the sequence and in turn only the 2Ph field and atomic coherence are generated. In the second stage of the sequence, where all the driving fields are present, we observe that both the 2Ph and 4Ph signals are correlated with the 2Ph signal emitted in the first stage.

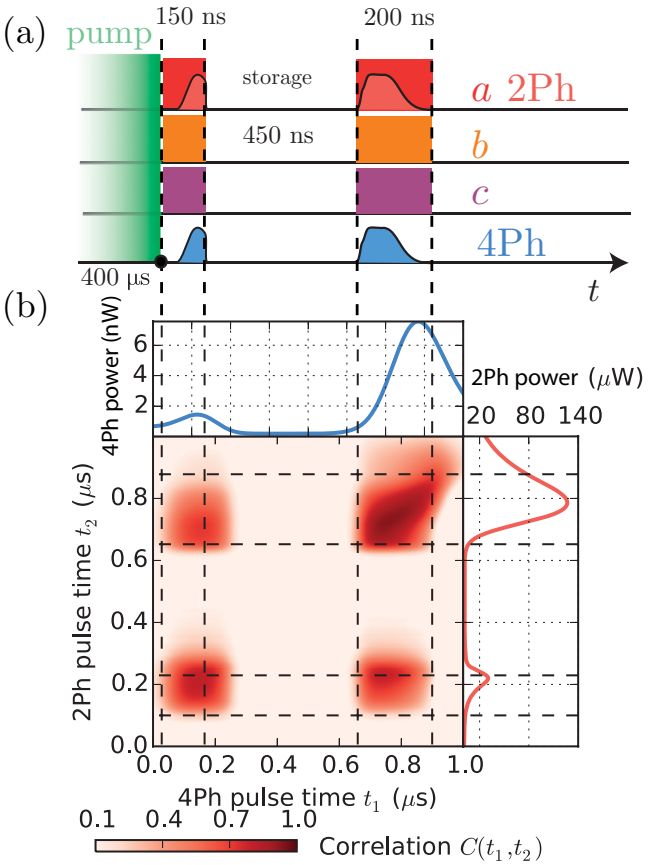

FIG. 4. (a) Scheme of experiment to demonstrate storage of ground-state atomic coherence for $\tau = 450$ ns. (b) Measured two-point correlation $C(t_1,t_2)$ between 2Ph and 4Ph signals with average registered signal powers. Off-diagonal elements of the correlation map demonstrate that light fields interact with the same atomic coherence before and after the time delay.

Agreement of the above measured statistics with theoretical predictions and multiple previous experiments proves that the correlations do arise from vacuum fluctuations. With driving power stable to within less than 1% and laser frequency stable to within 1 MHz, these external contributions to fluctuations can be neglected. Large magnitudes of fluctuations, with nearly perfect correlations between 2Ph and 4Ph signals, together with demonstrated storage of correlated signals allow one to reject phase-noise to amplitude-noise conversion as a source of correlations [38].

All of the above results were measured for $\Delta_g/2\pi = 1000$ MHz, $\Delta_h/2\pi = 1200$ MHz, and $\delta/2\pi = -50$ MHz.

B. Detuning dependence

Now we switch to verifying properties of the 4Ph signal for various drive field detunings. The influence of the field a detuning Δ_g is seen in Fig. 5. A number of pronounced effects comes about as this laser drives the Raman scattering and produces the ground-state atomic coherence ρ_{gh}. Initially the 2Ph signal grows exponentially. The corresponding Raman gain coefficient is strongly dependent on the drive field detuning Δ_g. The final effect is shortening of 2Ph pulses closer to resonance, as shown in Fig. 5(b). The 4Ph pulse follows the

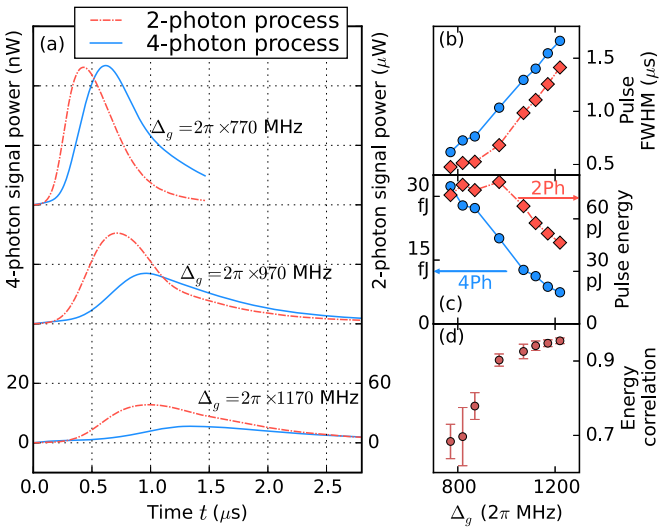

FIG. 5. (a) Averaged (over 500 realizations) pulse shapes for the intensities of the 2Ph and the 4Ph signals for a set of single-photon detunings Δ_g for constant $\delta/2\pi = -50$ MHz and $\Delta_h/2\pi = 1500$ MHz, (b) pulses full width at half maximum (FWHM), (c) their energies, and (d) pulse energy correlation between the two processes as a function of the field a single photon detuning Δ_g. Subsequent plots of 2Ph (4Ph) signals in panel (a) are shifted by 120 μW (40 nW).

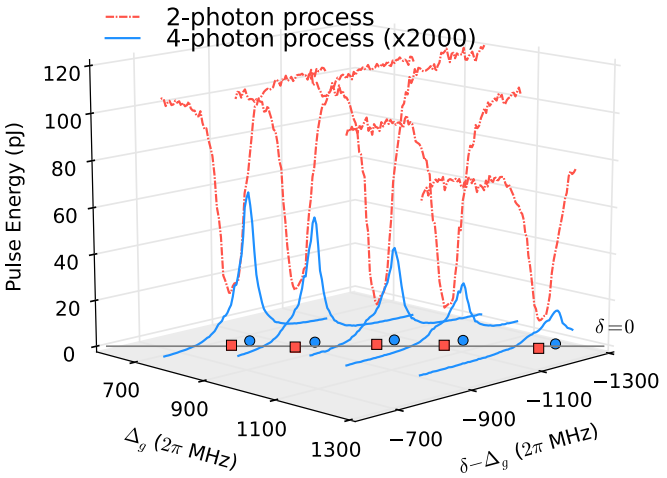

FIG. 6. Experimental average pulse energies of 2Ph and 4Ph signals as a function of the field a detuning Δ_g (measured from $F = 1 \rightarrow F' = 1$ resonance) and the field b detuning $\delta - \Delta_g$ around the two-photon resonance. As we change the field a detuning both the single-photon detuning Δ_g and the two-photon detuning δ change accordingly. Dots (squares) represent maxima (minima) of the 4Ph (2Ph) signal, while the $\delta = 0$ line indicates the two-photon absorption resonance.

ground-state coherence ρ_{gh} and the 2Ph pulse as shown in the previous section; however its maximum is somewhat delayed. We attribute this effect to internal atom dynamics at high drive intensity levels which is not captured by Eq. (1). The energies of pulses are also higher closer to resonance, although the two-photon Raman pulse energy saturates due to absorption losses [see Fig. 5(c)].

Important insight is provided by calculating the energy correlation between the 2Ph and 4Ph light pulses, which fluctuate significantly from shot to shot. The correlation is calculated as $C = \langle \Delta\mathcal{E}_{2\mathrm{Ph}} \Delta\mathcal{E}_{4\mathrm{Ph}} \rangle / \sqrt{\langle \Delta\mathcal{E}^2_{2\mathrm{Ph}} \rangle \langle \Delta\mathcal{E}^2_{4\mathrm{Ph}} \rangle}$, where $\mathcal{E}_{2\mathrm{Ph}}$ and $\mathcal{E}_{4\mathrm{Ph}}$ are the total energies of the 2Ph and 4Ph light pulses, respectively, in a single realization. The averaging $\langle \cdot \rangle$ is done over 500 realizations of the process and the results are plotted in Fig. 5(d). Strong correlations at various detunings reinforce the observation that indeed we are able to couple the 4Ph optical field to the ground-state coherence, since the number of photons in the 2Ph pulse is proportional to the generated atomic coherence $|\rho_{gh}|^2$. We attribute the drop in correlations close to the resonance line to absorption losses. Finally, we estimate the efficiency of conversion from the ground-state atomic coherence $\eta = \mathcal{E}_{4\mathrm{Ph}}/\mathcal{E}_{2\mathrm{Ph}}$ to the 4Ph field to be 5×10^{-4}. By comparing Eq. (1) with the analogous expression for the 2Ph process given by Eq. (4), we obtain $\eta \approx 10^{-4}$ as well. This figure of merit could be improved by choosing different experimental geometries or by laser cooling of the atomic ensemble.

To capture the physics in the vicinity of the two-photon resonance we study 4Ph and 2Ph pulse energies as a function of detunings of fields a and b. First we scan the field b detuning $\delta - \Delta_g$ across the two-photon resonance line (see Fig. 6). We observed strong suppression of the 2Ph signal (minima are marked by squares in Fig. 6) due to two-photon absorption (TPA) in the ladder configuration [39]. As a consequence, less atomic coherence ρ_{gh} is generated and the 4Ph signal is also reduced. In turn, the 4Ph shifted maxima position (marked by dots) are due to a trade-off between TPA losses and 4WM efficiency, as the latter is highest at the two-photon resonance (marked by the $\delta = 0$ line) according to Eq. (1). The peak appears only on one side of the resonance due to the phase-matching condition being influenced by atomic dispersion [40]. Additionally, we observe an expected broadening of 60 MHz of the two-photon resonance due to buffer gas collisions. By changing the field a detuning Δ_g we see the expected shifting of the two-photon resonance. We checked that even at suboptimal two-photon detuning δ the 2Ph and 4Ph signals are correlated, but the correlations become harder to measure as the 4Ph signals become very weak.

Contrary to the above, changing the detuning Δ_h of the 780-nm driving field c has only a mild effect on the 4Ph signal. Figure 7 presents the 4Ph signal pulse energy as a function of Δ_h while other lasers were tuned for maximal signal ($\Delta_g/2\pi = 900$ MHz and $\delta/2\pi = -50$ MHz). Since the 4Ph field frequency adapts to match the energy conservation for the $|h\rangle \rightarrow |e_3\rangle \rightarrow |e_2\rangle$ two-photon transition, the frequency of the driving field c is not critical. The laser must only be off-resonant, so the driving field is not absorbed and does not disturb the ground-state coherence. We also observe a marked narrow drop in the 4Ph process efficiency when the detuning between fields a and c is exactly the ground-state hyperfine splitting, or equivalently $\Delta_g + \Delta_h = 0$, which is due to Λ configuration two-photon resonance yielding strong interaction with the ground-state coherence.

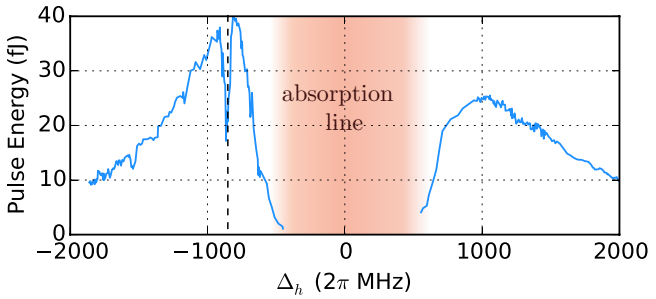

FIG. 7. Four-photon signal pulse energy as a function of the detuning Δ_h (measured from $F = 2 \rightarrow F' = 2$ resonance) of field c for optimal conditions of other lasers ($\Delta_g/2\pi = 900$ MHz and $\delta/2\pi = -50$ MHz). Absorption line corresponds to the $F = 2$ hyperfine component of the ground state, where the right side of the plot is the red-detuned side. Drop at around $\Delta_h/2\pi = -900$ MHz corresponds exactly to 6.8 GHz detuning between the two 780-nm lasers, or $\Delta_g + \Delta_h = 0$.

V. CONCLUSIONS

The experiment we performed is a proof-of-principle of a light atom interface that enables coupling of long-lived ground-state atomic coherence and light resonant with transition between excited states. The nonlinear process we discussed is a type of process with typical characteristics of both Raman scattering and 4WM. The observation of the inverted-Y-type nonlinear four-photon process involving ground-state coherence, performed in a very different regime in cold atoms, has been reported in Ref. [41]. Here, we generated ground-state atomic coherence via the well-known two-photon process. We demonstrated the ability to couple the very same atomic coherence to an optical field resonant with transition between two excited states via a four-photon process. This was verified by measuring high correlations between 2Ph and 4Ph fields, as well as by frequency and polarization characteristics of the four-photon process.

We studied the behavior of pulse shapes as a function of driving laser detunings. Among many results, we found that maximum signal is achieved when lasers are detuned from the two-photon resonance by approximately $\delta/2\pi = -50$ MHz, which is a trade-off between TPA spoiling the generation of atomic coherence and the efficiency of the four-photon process. This result demonstrates that we are able to control the 4WM process with ground-state coherence, which constitutes a type of Raman scattering driven by three nondegenerate fields, in analogy to hyper-Raman scattering where the scattering process is driven by two degenerate fields.

Here we used light at 776 nm coupled to the $5P_{3/2} \rightarrow 5D_{5/2}$ transition. Using different states, such as $4D_{3/2}$ as the highest excited state and $5P_{1/2}$ and $5P_{3/2}$ as two intermediate states, would enable coupling of telecom light (at 1475.7 or 1529.3 nm). Such a process could be used as a building block for a telecom quantum repeater or memory [5,14,18,19]. By applying an external weak quantum field as the 4Ph field, the system may serve as an atomic quantum memory, based on a highly nonlinear process as in Ref. [42], but still linear in the input field amplitude. It may also solve a variety of filtering problems [5,6], since many similar configurations exist (e.g., with $5P_{3/2}$, $5D_{3/2}$, and $5P_{1/2}$ as intermediate states) in which all driving lasers operate at different wavelengths than the signal. Even thought the 2Ph field was measured to be much stronger than the 4Ph field, we note that using a cold atomic ensemble would offer selectivity in intermediate states of the process and small detuning. Thanks to selection rules, exclusively the 4Ph process could be driven. This would be the requirement for generating pairs of photons and collective atomic excitations in the 4Ph process only. Additionally, the 4WM character of the process enables engineering of the phase-matching condition, namely, changing angles between incident driving beams to address different spin-wave excitations [4], to explore spatially multimode capabilities of the system. In future studies of the process we propose to address patterns unachievable by a typical Raman light-atom interface based on Λ-level configurations.

ACKNOWLEDGMENTS

We acknowledge R. Chrapkiewicz, M. Dąbrowski, and J. Nunn for insightful discussions and K. Banaszek and T. Stacewicz for their generous support. This work was supported by the Polish Ministry of Science and Higher Education under "Diamentowy Grant" No. DI2013 011943 and the National Science Centre under Grant No. DEC-2011/03/D/ST2/01941.

[1] C. H. van der Wal, M. D. Eisaman, A. André, R. L. Walsworth, D. F. Phillips, A. S. Zibrov, and M. D. Lukin, Science **301**, 196 (2003).

[2] M. Bashkansky, F. K. Fatemi, and I. Vurgaftman, Opt. Lett. **37**, 142 (2012).

[3] L. M. Duan, M. D. Lukin, J. I. Cirac, and P. Zoller, Nature (London) **414**, 413 (2001).

[4] R. Chrapkiewicz and W. Wasilewski, Opt. Express **20**, 29540 (2012).

[5] P. S. Michelberger, T. F. M. Champion, M. R. Sprague, K. T. Kaczmarek, M. Barbieri, X. M. Jin, D. G. England, W. S. Kolthammer, D. J. Saunders, J. Nunn, and I. A. Walmsley, New J. Phys. **17**, 043006 (2015).

[6] M. Dąbrowski, R. Chrapkiewicz, and W. Wasilewski, Opt. Express **22**, 26076 (2014).

[7] P. S. Donvalkar, V. Venkataraman, S. Clemmen, K. Saha, and A. L. Gaeta, Opt. Lett. **39**, 1557 (2014).

[8] F. E. Becerra, R. T. Willis, S. L. Rolston, and L. A. Orozco, Phys. Rev. A **78**, 013834 (2008).

[9] M. Parniak and W. Wasilewski, Phys. Rev. A **91**, 023418 (2015).

[10] A. A. M. Akulshin, R. J. R. McLean, A. I. Sidorov, and P. Hannaford, Opt. Express **17**, 22861 (2009).

[11] U. Khadka, H. Zheng, and M. Xiao, Opt. Express **20**, 6204 (2012).

[12] R. T. Willis, F. E. Becerra, L. A. Orozco, and S. L. Rolston, Phys. Rev. A **82**, 053842 (2010).

[13] B. Srivathsan, G. K. Gulati, B. Chng, G. Maslennikov, D. Matsukevich, and C. Kurtsiefer, Phys. Rev. Lett. **111**, 123602 (2013).
[14] T. Chanelière, D. N. Matsukevich, S. D. Jenkins, T. A. B. Kennedy, M. S. Chapman, and A. Kuzmich, Phys. Rev. Lett. **96**, 093604 (2006).
[15] J. M. Kondo, N. Šibalić, A. Guttridge, C. G. Wade, N. R. De Melo, C. S. Adams, and K. J. Weatherill, Opt. Lett. **40**, 5570 (2015).
[16] B. Huber, A. Kölle, and T. Pfau, Phys. Rev. A **90**, 053806 (2014).
[17] A. Kölle, G. Epple, H. Kübler, R. Löw, and T. Pfau, Phys. Rev. A **85**, 063821 (2012).
[18] W. Zhang, D.-S. Ding, S. Shi, Y. Li, Z.-Y. Zhou, B.-S. Shi, and G.-C. Guo, Phys. Rev. A **93**, 022316 (2016).
[19] A. G. Radnaev, Y. O. Dudin, R. Zhao, H. H. Jen, S. D. Jenkins, A. Kuzmich, and T. A. B. Kennedy, Nat. Phys. **6**, 894 (2010).
[20] M. G. Raymer and J. Mostowski, Phys. Rev. A **24**, 1980 (1981).
[21] M. D. Duncan, R. Mahon, L. L. Tankersley, and J. Reintjes, J. Opt. Soc. Am. B **7**, 1336 (1990).
[22] I. A. Walmsley, M. G. Raymer, T. Sizer, I. N. Duling, and J. D. Kafka, Opt. Commun. **53**, 137 (1985).
[23] M. Lewenstein, Z. Phys. B **56**, 69 (1984).
[24] M. Trippenbach and K. Rzążewski, Phys. Rev. A **31**, 1932 (1985).
[25] K. Zhang, J. Guo, C.-H. Yuan, L. Q. Chen, C. Bian, B. Chen, Z. Y. Ou, and W. Zhang, Phys. Rev. A **89**, 063826 (2014).
[26] M. G. Raymer, J. Mod. Opt. **51**, 1739 (2004).
[27] C. B. Wu, M. G. Raymer, Y. Y. Wang, and F. Benabid, Phys. Rev. A **82**, 053834 (2010).
[28] L. Q. Chen, G.-W. Zhang, C.-L. Bian, C.-H. Yuan, Z. Y. Ou, and W. Zhang, Phys. Rev. Lett. **105**, 133603 (2010).
[29] C.-H. Yuan, L. Q. Chen, J. Jing, Z. Y. Ou, and W. Zhang, Phys. Rev. A **82**, 013817 (2010).
[30] N. D. Zameroski, G. D. Hager, C. J. Erickson, and J. H. Burke, J. Phys. B **47**, 225205 (2014).
[31] M. G. Raymer, Z. W. Li, and I. A. Walmsley, Phys. Rev. Lett. **63**, 1586 (1989).
[32] X. Yang, J. Sheng, U. Khadka, and M. Xiao, Phys. Rev. A **85**, 013824 (2012).
[33] M. G. Raymer, K. Rzążewski, and J. Mostowski, Opt. Lett. **7**, 71 (1982).
[34] M. G. Raymer, I. A. Walmsley, J. Mostowski, and B. Sobolewska, Phys. Rev. A **32**, 332 (1985).
[35] I. A. Walmsley and M. G. Raymer, Phys. Rev. Lett. **50**, 962 (1983).
[36] R. Chrapkiewicz, W. Wasilewski, and C. Radzewicz, Opt. Commun. **317**, 1 (2014).
[37] M. Parniak and W. Wasilewski, Appl. Phys. B **116**, 415 (2014).
[38] L. S. Cruz, D. Felinto, J. Aguirre Gómez, M. Martinelli, P. Valente, A. Lezama, and P. Nussenzveig, Eur. Phys. J. D **41**, 531 (2006).
[39] H. S. Moon and H.-R. Noh, Opt. Express **21**, 7447 (2013).
[40] A. S. Zibrov, M. D. Lukin, L. Hollberg, and M. O. Scully, Phys. Rev. A **65**, 051801 (2002).
[41] D.-S. Ding, Z.-Y. Zhou, B.-S. Shi, X.-B. Zou, and G.-C. Guo, arXiv:1210.3963.
[42] R. A. de Oliveira, G. C. Borba, W. S. Martins, S. Barreiro, D. Felinto, and J. W. R. Tabosa, Opt. Lett. **40**, 4939 (2015).